University of Nebraska - Lincoln
DigitalCommons@University of Nebraska - Lincoln

Anthony F. Starace Publications | Research Papers in Physics and Astronomy

March 1980

# Photoionization of the 5*s* subshell of xenon: A multichannel *K*-matrix calculation including spin-orbit interactions

Keh-Ning Huang
*University of Nebraska - Lincoln*

Anthony F. Starace
*University of Nebraska-Lincoln*, astarace1@unl.edu

Follow this and additional works at: https://digitalcommons.unl.edu/physicsstarace

Part of the Physics Commons

Huang, Keh-Ning and Starace, Anthony F., "Photoionization of the 5*s* subshell of xenon: A multichannel *K*-matrix calculation including spin-orbit interactions" (1980). *Anthony F. Starace Publications*. 18.
https://digitalcommons.unl.edu/physicsstarace/18

This Article is brought to you for free and open access by the Research Papers in Physics and Astronomy at DigitalCommons@University of Nebraska - Lincoln. It has been accepted for inclusion in Anthony F. Starace Publications by an authorized administrator of DigitalCommons@University of Nebraska - Lincoln.

# Photoionization of the 5s subshell of xenon: A multichannel K-matrix calculation including spin-orbit interactions

Keh-Ning Huang* and Anthony F. Starace
*Behlen Laboratory of Physics, The University of Nebraska, Lincoln, Nebraska 68588*
(Received 16 October 1979)

*Ab initio* theoretical calculations are presented for the cross section, angular distribution, and spin polarization of photoelectrons for the 5s subshell of xenon. Starting from an initial basis of nonrelativistic Hartree-Fock wave functions, the authors treat the effect of final-state spin-orbit interaction in the Breit-Pauli approximation exactly. Electrostatic correlations between the 5s and 5p subshells are also included. Good agreement is obtained with experiment in the case of the photoionization cross section, but only qualitative agreement with experiment and with other theoretical calculations is obtained in the case of the photoelectron angular distribution due to the difficulty of obtaining accurate values for forbidden transition intensities starting from a nonrelativistic basis set. Spin polarization of as much as 20% is predicted near the 5s-subshell cross section minimum. Finally, some effects of the large discrepancies between Hartree-Fock and Dirac-Fock subshell binding energies and the corresponding experimental values are discussed.

## I. INTRODUCTION

The measurement of the angular distribution asymmetry parameter $\beta$ for the 5s subshell of xenon reported by Dehmer and Dill[1] was a striking demonstration of the importance of relativistic interactions to photoabsorption processes. The asymmetry parameter $\beta$ determines the differential photoionization cross section as follows[2]:

$$\frac{d\sigma}{d\Omega}=\frac{\sigma}{4\pi}[1+\beta P_2(\cos\theta)]\,,$$

where $\sigma$ is the total photoionization cross section and $\theta$ is measured from the direction of the polarization vector of the linearly polarized incident light. In general, $\beta$ is dependent on photon energy, due to interference between alternative final-state channels and takes values in the range $-1\leq\beta\leq+2$. Nonrelativistically, however, for s subshells of closed-shell atoms, there is only a *single* allowed final-state channel (i.e., $^1P$), and one may show that $\beta=2$ for all photon energies, implying that the photoelectron angular distribution[3] is $\cos^2\theta$. The measurement[1] of $\beta$ for the 5s subshell of xenon at 304 Å, however, gave the value $1.4\pm0.1$, indicating that relativistic interactions which permit transitions to the "forbidden" $^3P$ final state channel are quite significant.

The importance of spin-orbit interactions for the 5s subshell of xenon had been predicted earlier by Walker and Waber,[4] who presented theoretical independent-particle-model calculations in *jj* coupling using Dirac-Slater wave functions. The $\beta$ parameter was predicted to begin at $\approx-0.9$ at threshold, to increase rapidly to $\approx1.5$ at an energy 0.5 a.u. above threshold, and thereafter to rise slowly toward the value 2.0 at an energy 3.0 a.u. above threshold. However, Walker and Waber's use of an independent-electron model, implying the neglect of important electron correlations, gave a rather poor prediction for the 5s-subshell photoionization cross section.[4] Thus it was uncertain until the measurement reported by Dehmer and Dill[1] how significant are spin-orbit effects on photoabsorption processes such as the photoelectron angular distribution.

In this paper, we present *ab initio* calculations of the photoionization cross section, photoelectron angular distribution, and photoelectron spin polarization of the 5s subshell of xenon, taking proper account of both the final-state spin-orbit interaction and the strong correlations between the 5s subshell and the 5p subshell. The final-state spin-orbit interactions comprise both the spin-orbit interaction of the photoelectron in the field of the nucleus and the interactions induced by the mutual spin-orbit operator, which arises from the relativistic Breit-Pauli correction to the nonrelativistic Hartree-Fock Hamiltonian.[5] The spin-orbit interaction matrix elements were evaluated in terms of radial matrix elements using a graphical technique,[6,7] and the radial matrix elements were calculated using a basis set of *nonrelativistic* Hartree-Fock (HF) wave functions. The final-state spin-orbit and electrostatic perturbation matrix elements were then used to obtain the allowed $^1P$ and the forbidden $^3P$ dipole amplitudes for the Xe $5s\rightarrow\epsilon p$ transition by means of the K-matrix method.[8,9] Our predictions for the 5s-subshell photoionization cross section are in good agreement with experiment[10] in the region above threshold where the cross section has a minimum due to correlations between the 5p and 5s subshells. In this same energy region, however, our calculations pre-

 © 1980 The American Physical Society

dict a drop in $\beta$ to only a minimum value of $\approx 1.8$, considerably above the experimentally measured[1] value of $1.4 \pm 0.1$. We also report calculations indicating a substantial amount of photoelectron spin polarization in the vicinity of the minimum in the $5s$-subshell cross section. A preliminary report of our calculations has been presented elsewhere.[11]

While our calculation of the $5s$-subshell photoionization cross section has achieved good agreement with experiment, our calculation of $\beta$, whose deviation from the value 2 is a purely relativistic effect, has only been qualitatively successful. However, a comparison of our calculations, which employ a basis set of nonrelativistic HF wave functions, with recent calculations employing relativistic HF wave functions provides valuable information on the strength of relativistic effects in xenon and indicates some possible reasons for our limited success. The first of these recent relativistic calculations is that of Ong and Manson,[12,13] who have performed independent particle-model calculations employing Dirac-Fock wave functions. They obtain results for $\beta$ similar to those of Walker and Waber.[4] Johnson and Cheng[14,15] have carried out the most detailed calculations to date using the recently developed relativistic random-phase approximation.[16] They predict a minimum value for $\beta$ of about zero near the minimum in the $5s$ cross section. Their minimum value for $\beta$ is thus much lower than that obtained in our calculations, indicating a relative magnitude of the $^3P$ dipole amplitude that is about five times larger than ours. Detailed analysis and comparison of our results with those of Johnson and Cheng, presented below, indicate that the strength of the forbidden $^3P$ dipole transition amplitude is strongly dependent on the relativistic interactions within the xenon core and not just on the final state spin-orbit interactions included in our calculations. Lastly, Cherepkov[17] has made *ad hoc* modifications of previous nonrelativistic random-phase-approximation calculations[18] of the $^1P$ transition Xe $5s \to \epsilon p$ in order to fit the single data point[1] $\beta = 1.4 \pm 0.1$ at 304 Å. He predicts a minimum value for $\beta$ of $-1$ and a spin polarization having a maximum value of 100%. However, the magnitudes of these values are probably too great due to the unrealistic assumption of real dipole amplitudes; actually, the dipole amplitudes are complex numbers due to interchannel interactions.

In comparing our results with those of other calculations, we have also found that relaxation effects are quite significant. In particular, agreement between theory and experiment is found to be strongly dependent on whether the cross sections are plotted as a function of the photon energy or of the photoelectron energy. The differences between the two plots are caused by the discrepancies between theoretical and experimental values of the subshell binding energies in xenon. The importance of these and other relaxation effects has been known to theorists for some time,[19,20] but it is important that experimentalists are also aware of them. We discuss this influence of the binding energies on the $5s$-subshell photoabsorption processes in some detail.

In Sec. II we introduce the final-state spin-orbit and Coulomb interactions included in our calculations. In Sec. III we review briefly the multichannel $K$-matrix procedure for obtaining electric dipole transition amplitudes. In Sec. IV we summarize the theoretical formulas for experimentally measurable quantities in terms of these dipole amplitudes. In Sec. V we present and discuss our results, as well as those of others, for the dipole amplitudes, the photoionization cross sections, and the photoelectron angular distribution and spin polarization for the $5s$ subshell in xenon. Finally, Sec. VI summarizes our main conclusions.

## II. FINAL-STATE INTERACTION MATRIX

We have considered in this paper the spin-orbit and electrostatic interactions among the following four final-state channels:

$$\begin{aligned} \text{Xe}\, 5s^2 5p^6 + \hbar\omega \to \; & \text{Xe}^+ 5s^2 5p^5(^2P)\epsilon d(^1P_1) \\ & \text{Xe}^+ 5s5p^6(^2S)\epsilon p(^1P_1) \\ & \text{Xe}^+ 5s5p^6(^2S)\epsilon p(^3P_1) \\ & \text{Xe}^+ 5s^2 5p^5(^2P)\epsilon d(^3P_1) \end{aligned} \quad . \tag{1}$$

The final-state channels involving $5p \to \epsilon s$ transitions are ignored, since they have only a very minor effect on the $5s$-subshell cross section. Note also that the channels in Eq. (1) include the discrete members $np$ and $nd$ below the ionization thresholds. The bound-electron radial wave functions on the left and right of Eq. (1) were taken to be the neutral-xenon Hartree-Fock wave functions generated by Fischer's code.[21] The continuum HF wave functions on the right-hand side of Eq. (1) were calculated (using Bates' code[22] with nondiagonal Lagrangian multipliers[23]) in the $V^{N-1}$ HF potential[24] of the frozen xenon core. Using this basis of HF wave functions to represent the four final-state channels in Eq. (1) the final-state interaction matrix $V$ may be represented in block form as in Table I, which indicates the interactions that occur between each pair of channels. We discuss the interaction matrix $V$ in more detail below.

TABLE I. Block form of the final-state interaction matrix $V$. Each box indicates the interactions between each pair of final-state channels.

| | $(\epsilon d)\,^3P_1$ | $(\epsilon p)\,^3P_1$ | $(\epsilon p)\,^1P_1$ | $(\epsilon d)\,^1P_1$ |
|---|---|---|---|---|
| $(\epsilon d)\,^3P_1$ | Spin-orbit | Spin-orbit + Coulomb | Spin-orbit | Spin-orbit |
| $(\epsilon p)\,^3P_1$ | Spin-orbit + Coulomb | Spin-orbit | Spin-orbit | Spin-orbit |
| $(\epsilon p)\,^1P_1$ | Spin-orbit | Spin-orbit | 0 | Coulomb |
| $(\epsilon d)\,^1P_1$ | Spin-orbit | Spin-orbit | Coulomb | 0 |

### A. Spin-orbit matrix elements

The quantum-electrodynamic interaction between electrons can be approximated to the lowest order in the fine-structure constant $\alpha$ by the Breit interaction,[25,26] which in the Pauli approximation gives rise to the mutual spin-orbit interaction[5] (as well as others which are less important for the present purpose). Consequently, the total spin-orbit interaction for many-electron atoms can be written in atomic units as

$$V^{so}=\tfrac{1}{2}Z\alpha^2\sum_{i=1}^{N}\frac{1}{r_i^3}\vec{l}_i\cdot\vec{s}_i+\sum_{i\neq j}^{N}V_{ij}\,, \tag{2a}$$

where the mutual spin-orbit operator is

$$V_{ij}=-\tfrac{1}{2}\alpha^2\frac{1}{r_{ij}^3}(\vec{r}_{ij}\times\vec{p}_i)\cdot(\vec{s}_i+2\vec{s}_j)\,. \tag{2b}$$

Cases in which the mutual spin-orbit interaction can be reduced to an effective one-particle spin-orbit interaction have been enumerated.[6] For the present case the mutual spin-orbit interaction must be treated as a two-particle interaction. The evaluation of the spin-orbit matrix elements can be performed expediently by using graphical methods.[6,7] We present here only the results.

(a) The spin-orbit matrix elements between the $\epsilon p(^{2S+1}P_1)$ configurations with different continuum energies $\epsilon$ and different total spins $S$ are given by:

$$\langle Xe^+5s5p^6\epsilon' p(^{2S'+1}P_1)\,|\,V^{so}\,|\,Xe^+5s5p^6\epsilon p(^{2S+1}P_1)\rangle$$
$$=\begin{bmatrix}1 & \sqrt{2}\\ \sqrt{2} & 0\end{bmatrix}(-\tfrac{1}{2}\zeta_{\epsilon'\epsilon}+\eta_{\epsilon'\epsilon})+\begin{bmatrix}3A-B-C & -\sqrt{2}A-\frac{1}{3}\sqrt{2}(B-C)\\ -\sqrt{2}A+\frac{1}{3}\sqrt{2}(B-C) & 0\end{bmatrix}. \tag{3}$$

In (3), the first (second) column and row are for the triplet (singlet), and we have defined

$$\zeta_{\epsilon'\epsilon}=\frac{Z\alpha^2}{2}\int_0^\infty dr\,P_{\epsilon' p}(r)P_{\epsilon p}(r)\frac{1}{r^3}\,, \tag{4}$$

$$\begin{aligned}\eta_{\epsilon'\epsilon}=\sum_{n}^{\text{closed}}\;&[N^0(\epsilon' pns;\epsilon pns)-K^1(\epsilon' pns;ns\epsilon p)+3N^0(\epsilon' pnp;\epsilon pnp)-\tfrac{9}{5}K^2(\epsilon' pnp;np\epsilon p)-\tfrac{21}{5}N^0(\epsilon' pnp;np\epsilon p)\\&+\tfrac{9}{5}N^2(\epsilon' pnp;np\epsilon p)+5N^0(\epsilon' pnd;\epsilon pnd)+K^1(\epsilon' pnd;nd\epsilon p)-\tfrac{18}{7}K^3(\epsilon' pnd;nd\epsilon p)+3N^{-1}(\epsilon' pnd;nd\epsilon p)\\&-\tfrac{69}{7}N^1(\epsilon' pnd;nd\epsilon p)+\tfrac{36}{7}N^3(\epsilon' pnd;nd\epsilon p)+(\epsilon' p\longleftrightarrow\epsilon p)]\,,\end{aligned} \tag{5}$$

and

$$A=N^0(\epsilon' p5s;\epsilon p5s)\,, \tag{6a}$$

$$B=K^1(\epsilon' p5s;5s\epsilon p)\,, \tag{6b}$$

$$C=K^1(\epsilon p5s;5s\epsilon' p)\,. \tag{6c}$$

The summation in (5) is over all closed subshells, and the symbol $(\epsilon' p\longleftrightarrow\epsilon p)$ denotes additional terms with $\epsilon' p$ and $\epsilon p$ interchanged for all terms listed explicitly. The radial integrals used in (5) and (6) are defined by

$$N^l(ab;cd)=\frac{\alpha^2}{4}\int_0^\infty dr_1\int_0^\infty dr_2\,P_a(r_1)P_b(r_2)\times\frac{r_2^l}{r_1^{l+3}}\theta(r_1-r_2)P_c(r_1)P_d(r_2)\,, \tag{7}$$

$$K^l(ab;cd)=\frac{\alpha^2}{4}\int_0^\infty dr_1\int_0^\infty dr_2\,P_a(r_1)P_b(r_2)\times\frac{r_<^l}{r_>^{l+1}}\frac{1}{r_1}\left(\frac{d}{dr_1}-\frac{1}{r_1}\right)P_c(r_1)P_d(r_2)\,. \tag{8}$$

A more general formula which reduces to (3) in a special case has been obtained previously.[6]

(b) The spin-orbit matrix elements between the $\epsilon d(^{2S+1}P_1)$ configurations with different continuum energies $\epsilon$ and different total spins $S$ are

$$\langle Xe^+5s^25p^5\epsilon' d(^{2S'+1}P_1)\,|\,V^{so}\,|\,Xe^+5s^25p^5\epsilon d(^{2S+1}P_1)\rangle=-\tfrac{1}{4}\zeta_{5p5p}\begin{bmatrix}1 & -\sqrt{2}\\ -\sqrt{2} & 0\end{bmatrix}\delta(\epsilon-\epsilon')-\tfrac{3}{4}\zeta_{\epsilon'd\epsilon d}\begin{bmatrix}1 & \sqrt{2}\\ \sqrt{2} & 0\end{bmatrix}, \tag{9}$$

where the $\delta$ function $\delta(\epsilon-\epsilon')$ indicates that the $5p$-subshell spin-orbit interaction occurs only for states diagonal in the photoelectron energy $\epsilon$. The parameters $\zeta$ in Eq. (9) are given by expressions similar to that in Eq. (4).

(c) The spin-orbit matrix elements between configurations $\epsilon p(^{2S+1}P_1)$ and $\epsilon' d(^{2S'+1}P_1)$ are given by

$$\langle \mathrm{Xe}^+ 5s^2 5p^5 \epsilon d(^{2S'+1}P_1)\,|\,V^{so}\,|\,\mathrm{Xe}^+ 5s5p^6\epsilon p(^{2S+1}P_1)\rangle = \begin{bmatrix} \frac{1}{3\sqrt{2}}D & -D+F \\ -D+G & 0 \end{bmatrix}, \quad (10)$$

where

$$D=-N^{-1}(5s\epsilon d;5p\epsilon p)+5N^1(\epsilon d5s;\epsilon p5p)+K^1(\epsilon d5s;\epsilon p5p)-K^1(5p\epsilon p;5s\epsilon d)\,, \quad (11a)$$

$$F=\tfrac{4}{3}[3K^1(\epsilon d5s;5p\epsilon d)+K^1(5p\epsilon p;\epsilon d5s)+K^1(\epsilon p5p;5s\epsilon d)]\,, \quad (11b)$$

$$G=\tfrac{2}{3}[3K^1(\epsilon d5s;5p\epsilon d)+K^1(5p\epsilon p;\epsilon d5s)+4K^1(\epsilon p5p;5s\epsilon d)]\,. \quad (11c)$$

### B. Coulomb matrix elements

Owing to our use of HF basis wave functions the only sub-blocks of the matrix $V$ having nonzero electrostatic-interaction matrix elements are those between $\epsilon p(^{2S+1}P_1)$ and $\epsilon' d(^{2S+1}P_1)$ for $S=0$ and 1. These matrix elements may be written in terms of Slater integrals as follows:

$$\langle \mathrm{Xe}^+ 5s5p^6\epsilon p(^{2S+1}P_1)\left|\sum_{i>j}\frac{1}{r_{ij}}\right|\mathrm{Xe}^+ 5s^2 5p^5\epsilon d(^{2S+1}P_1)\rangle=\delta_{S0}\tfrac{2}{3}\sqrt{2}\,R^1(5s\epsilon d;\epsilon p5p)-\tfrac{1}{3}\sqrt{2}\,R^1(5s\epsilon d;5p\epsilon p)\,. \quad (12)$$

## III. MULTICHANNEL $K$-MATRIX CALCULATION OF IMPROVED DIPOLE MATRIX ELEMENTS

Our aim is to calculate the exact energy eigenstates of the Hamiltonian given by

$$H=H_{\mathrm{HF}}+V\,,$$

where $H_{\mathrm{HF}}$ is the HF Hamiltonian, within the subspace of the four final-state channels in Eq. (1). We note, however, that the part of $V$ proportional to a $\delta$ function [cf. Eq. (9)] should be diagonalized first. This diagonalization results in a linear transformation of the $\epsilon d(^{2S+1}P_1)$ channels into two new final-state channels having slightly different binding energies (corresponding to the fine-structure splitting of the $5p^5$ ionic core). Our new states $|\lambda\epsilon\rangle$ may be written as follows:

$$\begin{aligned} |1\epsilon\rangle&=(\tfrac{1}{3})^{1/2}|\epsilon d\,^1P_1\rangle-(\tfrac{2}{3})^{1/2}|\epsilon d\,^3P_1\rangle\,,\\ |2\epsilon\rangle&=|\epsilon p\,^3P_1\rangle,\quad |3\epsilon\rangle=|\epsilon p\,^1P_1\rangle\,,\\ |4\epsilon\rangle&=(\tfrac{2}{3})^{1/2}|\epsilon d\,^1P_1\rangle+(\tfrac{1}{3})^{1/2}|\epsilon d\,^3P_1\rangle\,. \end{aligned} \quad (13)$$

Within the new basis set the interaction matrix $V$ has the form

$$\langle\lambda\epsilon\,|\,V\,|\,\lambda'\epsilon'\rangle=V_\lambda\delta_{\lambda\lambda'}\delta(\epsilon-\epsilon')+\langle\lambda\epsilon\,|\,V'\,|\,\lambda'\epsilon'\rangle\,, \quad (14)$$

where $V_\lambda=0$ (for $\lambda=2,3$) and $V_\lambda\neq 0$ (for $\lambda=1,4$) and where $V'$ is the part of $V$ that is not proportional to a $\delta$ function. The eigenvalues $V_\lambda$ serve to shift the binding energy of the $\lambda$th channel and thus may be grouped with $H_{\mathrm{HF}}$ to form a new zero-order Hamiltonian

$$\begin{aligned}\langle\lambda'\epsilon'\,|H_0|\,\lambda\epsilon\rangle&=\langle\lambda'\epsilon'\,|H_{\mathrm{HF}}|\,\lambda\epsilon\rangle+V_\lambda\delta_{\lambda'\lambda}\delta(\epsilon'-\epsilon)\\ &=\delta_{\lambda'\lambda}\delta(\epsilon-\epsilon')(\epsilon+I_\lambda+V_\lambda)\,, \end{aligned} \quad (15)$$

where $\epsilon$ is the photoelectron kinetic energy and $I_\lambda$ is its binding energy in the state $|\lambda\epsilon\rangle$. (We shall denote kinetic energies by $\epsilon$ and total energies with respect to some zero by $E$; in this paper our zero of energy was chosen to be the $5p$-subshell ionization threshold.) The usual $K$-matrix theory may now be applied to the Hamiltonian $H$ defined by

$$H=H_0+V'\,. \quad (16)$$

The incoming-wave normalized energy eigenstates of the Hamiltonian in Eq. (16) within the subspace of states given by Eq. (13) may be written in terms of the reaction matrix $K(E)$ of scattering theory as follows[8,9]:

$$|\lambda E-\rangle=\sum_{\lambda'}\left(|\lambda' E\rangle+\sum_{\lambda''}\mathcal{P}\int\frac{dE''\,|\,\lambda''E''\rangle\langle\lambda''E''\,|\,K(E)\,|\,\lambda' E\rangle}{E-E''}\right)C_{\lambda'\lambda} \quad (17a)$$

where

$$C_{\lambda'\lambda}\equiv\sum_{\Lambda}U_{\lambda'\Lambda}\cos\eta_\Lambda\exp(-i\eta_\Lambda)\times\tilde{U}_{\Lambda\lambda}\exp(-i\delta_\lambda)\,. \quad (17b)$$

In Eq. (17a) the symbol $\mathcal{P}$ indicates that the Cauchy

principal part is to be taken when integrating over the singularity in the denominator, and the integration over the final-state energy $E''$ implies also a summation over discrete states. The reaction matrix in Eq. (17a) is obtained as the solution of the following integral equation:

$$\langle\lambda' E'|K(E)|\lambda E\rangle = \langle\lambda' E'|V'|\lambda E\rangle + \sum_{\lambda''} \mathcal{P}\int dE'' \frac{\langle\lambda' E'|V'|\lambda'' E''\rangle\langle\lambda'' E''|K(E)|\lambda E\rangle}{E-E''}. \tag{18}$$

The orthogonal matrix $U_{\lambda\Lambda}(E)$, which transforms the zero-order channels $\lambda$ to eigenchannels $\Lambda$ at fixed energy $E$, as well as the eigenphase shifts $\eta_\Lambda$, which are due to the interactions between states $|\lambda\epsilon\rangle$, are obtained by diagonalizing the on-the-energy-shell $K$ matrix, as follows:

$$\sum_{\lambda'} \langle\lambda E|K(E)|\lambda' E\rangle U_{\lambda'\Lambda} = -\pi^{-1}\tan(\eta_\Lambda) U_{\lambda\Lambda}. \tag{19}$$

In Eq. (19) $-\pi^{-1}\tan\eta_\Lambda$ is the $\Lambda$th eigenvalue. Finally, the phase shift $\delta_\lambda$ in Eq. (17b) is the phase shift of the zero-order states $|\lambda\epsilon\rangle$ with respect to Coulomb waves; for $\lambda = 2, 3$ this phase shift is simply the HF phase shift with respect to Coulomb waves.[27] The phase factors appearing in Eq. (17b) are required to convert the standing-wave normalization to incoming-wave normalization as required for photoionization processes.[9,28,29]

Electric-dipole-transition amplitudes may be obtained by taking matrix elements of the length form of the dipole operator, $\sum_i \vec{r}_i$, between the initial state $\langle 0|$, where

$$\langle 0| \equiv \langle \mathrm{Xe}\ 1s^2 \ldots 5s^2 5p^6 (^1S_0)|, \tag{20}$$

and the final state $|\lambda E-\rangle$ given in Eq. (17). The reduced dipole amplitudes (length form) are given by

$$\langle 0\| \sum_{i=1}^{N} r_i^{(1)} \| \lambda E-\rangle = D(\lambda E)\exp(-i\delta_{\lambda E}), \tag{21}$$

where

$$D(\lambda E) = \sum_{\lambda'}\left(\left\langle 0\| \sum_{i=1}^{N} r_i^{(1)} \| \lambda' E\right\rangle + \sum_{\lambda''} \mathcal{P}\int dE'' \frac{\left\langle 0\| \sum_{i=1}^{N} r_i^{(1)} \| \lambda'' E\right\rangle \langle\lambda'' E|K(E)|\lambda' E\rangle}{E-E''}\right) \sum_{\lambda} U_{\lambda'\Lambda}\cos(\eta_\Lambda)\exp(-i\eta_\Lambda)\bar{U}_{\Lambda\lambda}. \tag{22}$$

The zero-order reduced dipole amplitudes

$$\left\langle 0\| \sum_{i=1}^{N} r_i^{(1)} \| \lambda' E\right\rangle$$

are given in terms of the HF reduced dipole amplitudes by using the transformation in Eq. (13), and noting that

$$\left\langle 0\| \sum_{i=1}^{N} r_i^{(1)} \| \epsilon d\, {}^1P_1\right\rangle = -2\int_0^\infty P_{5p}(r) r P_{\epsilon d}(r)\, dr, \tag{23a}$$

$$\left\langle 0\| \sum_{i=1}^{N} r_i^{(1)} \| \epsilon p\, {}^1P_1\right\rangle = -\sqrt{2}\int_0^\infty P_{5s}(r) r P_{\epsilon p}(r)\, dr, \tag{23b}$$

$$\left\langle 0\| \sum_{i=1}^{N} r_i^{(1)} \| \epsilon l\, {}^3P_1\right\rangle = 0 \quad \text{for } l = 1, 2. \tag{23c}$$

Similar expressions may be given for the velocity form of the electric-dipole operator $\sum_{i=1}^{N} \vec{\nabla}_i$:

$$\left\langle 0\| \sum_{i=1}^{N} \nabla_i^{(1)} \| \lambda E-\right\rangle = \bar{D}(\lambda E-)\exp(-i\delta_{\lambda E}), \tag{24}$$

where $\bar{D}(\lambda E-)$ is given by an equation similar to Eq. (22) (with $r_i^{(1)}$ replaced by $\nabla_i^{(1)}$ everywhere). The two nonzero HF reduced dipole amplitudes in the velocity form are:

$$\left\langle 0\| \sum_{i=1}^{N} \nabla_i^{(1)} \| \epsilon d\, {}^1P_1\right\rangle = -2\int_0^\infty r^2 dr\, R_{5p}(r)\left(\frac{d}{dr}+\frac{3}{r}\right) R_{\epsilon d}(r), \tag{25a}$$

$$\left\langle 0\| \sum_{i=1}^{N} \nabla_i^{(1)} \| \epsilon p\, {}^1P_1\right\rangle = -\sqrt{2}\int_0^\infty r^2 dr\, R_{5s}(r)\left(\frac{d}{dr}+\frac{2}{r}\right) R_{\epsilon p}(r). \tag{25b}$$

Note that in the absence of final-state interaction (i.e., $V = K = 0$, $\eta_\Lambda = 0$, and $U_{\lambda\Lambda} = \delta_{\lambda\Lambda}$) the improved dipole amplitude $D(\lambda E-)$ reduces to the real, zero-order dipole amplitude:

$$\lim_{V\to 0} D(\lambda E-) = \left\langle 0\| \sum_{i=1}^{N} r_i^{(1)} \| \lambda E\right\rangle. \tag{26}$$

We have factored out the zero-order phase $\exp(-i\delta_{\lambda E})$ in Eq. (21) in order to facilitate the

comparison between $D(\lambda E-)$ and $\langle 0 \| \sum_{i=1}^{N} r_i^{(1)} \| \lambda E\rangle$. Furthermore, as shown in Sec. IV, the formulas for the cross section and the asymmetry parameter for the 5s subshell in xenon do not depend on $\delta_{\lambda E}$, but only on $D(\lambda E-)$.

The procedure, then, for obtaining improved dipole amplitudes is as follows. First one solves the integral equation (18) by reduction to a set of linear algebraic equations,[30] using the interaction matrix $V$ calculated as in Section II. Then one calculates the zero-order HF reduced dipole matrix elements according to either the length form in Eq. (23) or the velocity form in Eq. (25). Improved reduced dipole amplitudes are obtained by transforming the HF amplitudes according to Eqs. (13), (21), and (22).

## IV. FORMULAS FOR EXPERIMENTALLY MEASURABLE QUANTITIES

All experimentally measurable quantities related to photoionization of the 5s subshell of xenon near its threshold may be expressed theoretically in terms of the effective reduced dipole matrix elements given by Eqs. (21) and (22). Since we shall be interested only in the 5s subshell, the channel index $\lambda$ will have the values 2 and 3 [cf. Eq. (13)] corresponding to the $^3P$ and $^1P$ final states of the transition $5s \to \epsilon p$. For greater clarity and simplicity, we shall in what follows replace the index $\lambda$ by $^{2S+1}P$ where $S=0,1$. Thus, the effective dipole amplitude $D(\lambda E)$ and the HF phase shift $\delta_{\lambda E}$ in Eqs. (21) and (22) will now be referred to simply by $D_E(^{2S+1}P)$ and $\delta_E(^{2S+1}P)$. Formulas for the photoionization cross section, photoelectron angular distribution, and photoelectron spin polarization are discussed in turn below.

### A. Photoionization cross section

The cross section for photoionization of the 5s subshell in Xe is given in atomic units by

$$\sigma(\omega)=\frac{4\pi^2}{3c}\omega[\,|D_E(^1P)|^2+|D_E(^3P)|^2]\,. \tag{27}$$

In Eq. (27) $\omega$ is the photon energy in atomic units (1 a.u. = 27.2108 eV) and $4\pi^2/3c = 2.68909\times10^{-18}$ cm$^2$. In theoretical photoionization calculations, of course, specification of the photon energy is only part of the information needed to calculate dipole amplitudes. One needs to know also the photoelectron kinetic energies since these are the energies which determine the properties of (23)]. The kinetic energies $\epsilon_{5s}$ and $\epsilon_{5p}$ of electrons ejected from the 5s and 5p subshells are related to the photon energy $\omega$ by

$$\omega=\begin{cases} I_{5s}+\epsilon_{5s} & \text{(28a)}\\ I_{5p}+\epsilon_{5p} & \text{(28b)}\end{cases}$$

TABLE II. Comparison of theoretical and experimental binding energies for the outer subshells of Xe (in a.u.).

| Source | $I_{5p}$ [e] | $I_{5s}$ | $I_{5s}-I_{5p}$ |
|---|---|---|---|
| Hartree-Fock [a] | 0.4634 | 0.9444 | 0.4810 |
| Dirac-Fock [b] | 0.4574 | 1.0102 | 0.5528 |
| Dirac-Fock plus relaxation and correlation [c] | 0.4627 | 0.8482 | 0.3855 |
| Experiment [d] | 0.4618 | 0.8598 | 0.3980 |

[a] E. Clementi and C. Roetti, Ref. 31.
[b] J. P. Desclaux, Ref. 32.
[c] M. Aoyagi *et al.*, Ref. 33(a) and K.-N. Huang *et al.*, Ref. 33(b).
[d] C. E. Moore, Ref. 34.
[e] $\langle I_{5p}\rangle = \frac{2}{3} I_{5p}(J=\frac{3}{2}) + \frac{1}{3} I_{5p}(J=\frac{1}{2})$.

where $I_{5s}$ and $I_{5p}$ are the subshell binding energies. A number of theoretical[31-33] values for $I_{5s}$ and $I_{5p}$ as well as the experimental[34] values are shown in Table II. We see that the HF[31] and the Dirac-Fock[32] theoretical binding energies, particularly for the 5s subshell, differ substantially from the experimental values. Good theoretical binding energies can be obtained, but to do so one must include relaxation and electron correlation effects for inner shells.[33] Use of the HF or Dirac-Fock binding energies, rather than experimental energies, affects the theoretically predicted cross sections in two ways. Firstly, the photon energy $\omega$ at which the onset of photoionization occurs is incorrect [cf. Eq. (28)]. Thus the cross section value at threshold is incorrect, due to its proportionality to $\omega$. In addition, if the theoretical cross section is plotted vs photon energy, rather than vs photoelectron kinetic energy, then the theoretical cross section for a given subshell will appear shifted in energy with respect to the experimental cross section for the same subshell. Secondly, if the theoretical calculation takes into account intersubshell correlations, then the relative binding energies between subshells will affect the strength of electron correlations through the energy denominators involved in the calculations [cf. Eqs. (18) and (22)].

### B. Photoelectron angular distribution asymmetry parameter $\beta$

In an $LS$-coupling representation, the angular-momentum-transfer formulation for $\beta$ shows that the $^1P$ and $^3P$ amplitudes combine incoherently as follows[35]:

$$\beta(E)=\frac{2|D_E(^1P)|^2-|D_E(^3P)|^2}{|D_E(^1P)|^2+|D_E(^3P)|^2}\,. \tag{29}$$

If we define the $^3P/^1P$ cross section ratio $r$,

TABLE III. Relation between the asymmetry parameter $\beta$ and the $^3P/^1P$ cross section ratio $r$.

| | | | | | | | | |
|---|---|---|---|---|---|---|---|---|
| $\beta$ | 2.0 | 1.8 | 1.4 | 1.0 | 0.6 | 0.2 | 0.0 | −1.0 |
| $r$ | 0.0 | 0.071 | 0.25 | 0.5 | 0.875 | 1.5 | 2.0 | $\infty$ |

where

$$r \equiv |D_E(^3P)|^2/|D_E(^1P)|^2, \tag{30}$$

then $\beta$ is seen to depend only on $r$:

$$\beta = (2-r)/(1+r). \tag{31}$$

In Table III we have given several values of $\beta$ and $r$, as related by Eq. (31). We see that $\beta = 2$ when $r = 0$, corresponding to $D(^3P) = 0$, and $\beta = -1$ only when $r = \infty$, corresponding to $D(^1P) = 0$. The experimental value[1] for $\beta$ at 304 Å is 1.4, which corresponds to a value for $r$ of 0.25.

### C. Photoelectron spin polarization

General discussions of photoelectron spin polarization have been given recently by Brehm,[36] Jacobs,[37] Cherepkov,[38] Lee,[39] and Huang.[40] We use here the notation of Huang[40] and consider specifically the case of photoelectrons ejected by circularly polarized light incident on an unpolarized gas. The geometrical relationships are shown in Fig. 1, where $Z$ is the direction of the incident circularly polarized light and $z$ is the direction of the photoelectron. The electron spin polarization along the $x$, $y$, $z$, and $Z$ directions (where $x$ is the direction of increasing $\theta$ and $y$ is the direction of increasing $\phi$) is given by[40,41]:

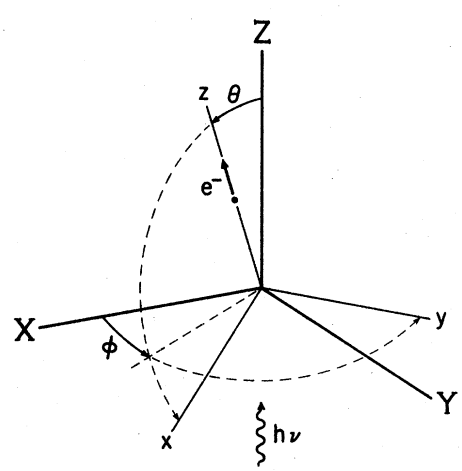


FIG. 1. Geometrical relationships used in spin polarization formulas. Circularly polarized light is incident along the $Z$ axis. The photoelectron is ejected along the $z$ axis.

$$P_x(\theta,\phi) = \frac{\pm\xi \sin\theta}{1 - \frac{1}{2}\beta P_2(\cos\theta)}, \tag{32}$$

$$P_y(\theta,\phi) = \frac{\eta \sin\theta \cos\theta}{1 - \frac{1}{2}\beta P_2(\cos\theta)}, \tag{33}$$

$$P_3(\theta,\phi) = \frac{\pm\zeta \cos\theta}{1 - \frac{1}{2}\beta P_2(\cos\theta)}, \tag{34}$$

$$P_Z(\theta,\phi) = P_z(\theta,\phi)\cos\theta - P_x(\theta,\phi)\sin\theta. \tag{35}$$

In Eqs. (32) and (34) the + (−) sign applies to right (left) circularly polarized incident light. The parameters $\xi$, $\eta$, and $\zeta$ for the 5s subshell of xenon are given in terms of the dipole amplitudes in Eq. (21) above as follows[40]:

$$\xi = \frac{\frac{3}{4}\sqrt{2}\,[D_E^*(^1P)D_E(^3P)\exp i(\delta_E(^1P) - \delta_E(^3P)) + \text{c.c.}]}{|D_E(^1P)|^2 + |D_E(^3P)|^2}, \tag{36}$$

$$\eta = \frac{-i\frac{3}{4}\sqrt{2}\,[D_E^*(^1P)D_E(^3P)\exp i(\delta_E(^1P) - \delta_E(^3P)) - \text{c.c.}]}{|D_E(^1P)|^2 + |D_E(^3P)|^2}, \tag{37}$$

$$\zeta = \frac{\frac{3}{2}|D_E(^3P)|^2}{|D_E(^1P)|^2 + |D_E(^3P)|^2}. \tag{38}$$

If $P_Z(\theta,\phi)$ is integrated over all angles, one obtains the total spin polarization along the $Z$ axis:

$$P = \sigma^{-1}\int P_Z(\theta,\phi)\frac{d\sigma}{d\Omega}\,d\Omega = \pm\frac{(\zeta - 2\xi)}{3}. \tag{39}$$

Spin polarization in other directions vanishes. For arbitrarily polarized incident light, the photoelectron spin polarization formulas (32), (33), (34), and (39) must be modified,[40] but they are still characterized by the three parameters $\xi$, $\eta$, and $\zeta$.

## V. RESULTS AND DISCUSSION

### A. Photoionization cross section

Our theoretical results for the 5s-subshell photoionization cross section are shown by the two solid lines in Fig. 2. The results are plotted vs photoelectron energy so that theoretical and experimental thresholds coincide. We have used theoretical HF binding energies in our calculations. Not shown, for clarity, are our zero-order HF results, which have the following well-known behavior.[42,43] The length (velocity) cross section is only 0.05 Mb (0.01 Mb) at threshold, but rises to a maximum value of 0.27 Mb (0.17 Mb) at an energy 0.7 a.u. above threshold, whereupon it decreases monotonically for higher energies. Our solid curves in Fig. 2 take into account the influence of $5p \to \epsilon d$ transitions on the $5s \to \epsilon p$ transitions, thereby demonstrating the well-known interference that leads to a cross section

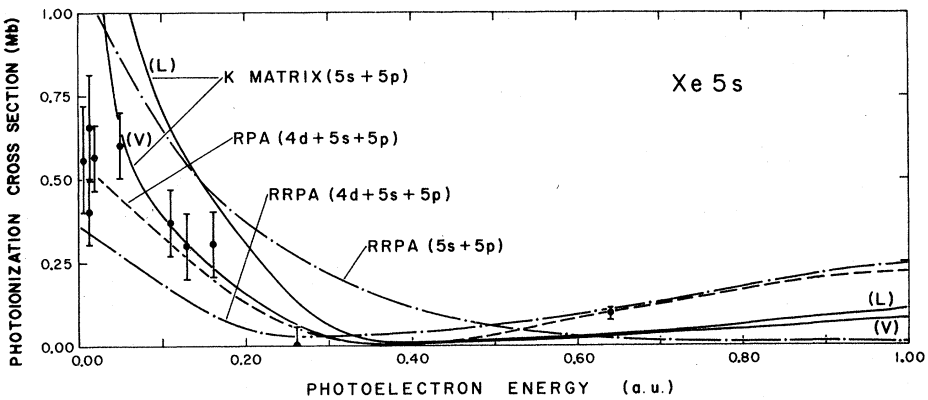


FIG. 2. Photoionization cross section for the 5$s$ subshell of xenon plotted vs photoelectron energy. Solid curves: present $K$-matrix results in length ($L$) and velocity ($V$) approximation. Dot-dashed lines: relativistic-random-phase-approximation (RRPA) calculations of Johnson and Cheng (Refs. 14 and 15). Dashed line: random-phase-approximation (RPA) calculations of Amusia and Cherpkov (Ref. 18). Solid circles: experimental measurements of Samson and Gardner (Ref. 10). Note that for each of the theoretical calculations we have indicated in parenthesis the subshells among which final-state correlations are included.

minimum at about 0.4 a.u. above threshold.[43] We have neglected the weaker interaction between the $5s \to \epsilon p$ transitions and the $5p \to \epsilon s$ transitions, which may slightly modify the position of our cross-section minimum.

The experimentally measured cross sections of Samson and Gardner[10] are also shown in Fig. 2. Our calculated cross sections are much higher than the experimental measurements at threshold, where our length (velocity) cross sections have the value 3.8 Mb (2.0 Mb). However, our velocity cross section is in good agreement with experiment for photoelectron energies in the range $0.05 \leq \epsilon \leq 0.3$ a.u. In this energy region the length cross section is higher than the velocity cross section by a factor of 2. Above the minimum in the cross section our results rise slightly, but not as rapidly as the experimental measurement at $\epsilon = 0.64$ a.u. We note that Gustafsson[44] has measured the photoionization cross section in the vicinity of the cross section minimum. However, his results are sensitive to the photoelectron angular distribution,[44] which is shown below to be rapidly varying in the same energy region. For this reason we have not plotted these measurements.

The RPA cross section of Amusia and Cherepkov,[18] which employs experimental ionization thresholds, and the relativistic RPA cross sections of Johnson and Cheng,[14,15] which employ Dirac-Fock ionization thresholds, are also shown in Fig. 2. The relativistic RPA calculation including only 5$s$ and 5$p$ subshell interactions [i.e., RRPA ($5s + 5p$)] is qualitatively similar to our own results: it gives too high a cross section at threshold and it fails to rise significantly at higher energies. However, unlike our $K$-matrix calculation, the RRPA ($5s + 5p$) cross section fails to give a minimum in the cross section in the expected energy region, i.e., near $\epsilon = 0.4$ a.u. Whereas both our $K$-matrix calculation and the RRPA ($5s + 5p$) calculation consider all major final-state correlations between the 5$s$ and 5$p$ subshells as well as final-state spin-orbit interactions, there are the following differences. We have used nonrelativistic HF core wave functions and binding energies, whereas the RRPA calculations use Dirac-Fock core wave functions and binding energies. In addition, all of the RPA calculations take into account certain ground-state correlation effects not included in our $K$-matrix calculations. Lastly we have ignored interactions between the 5$s$ subshell and the relatively weak $5p \to \epsilon s$ transitions. The RPA calculation of Amusia and Cherepkov[18] as well as the RRPA ($4d + 5s + 5p$) calculation achieve much better agreement with experiment at threshold and at high energy, due, apparently, to their inclusion of final-state correlation between the 5$s$ and 4$d$ subshells (as well as that between the 5$s$ and 5$p$ subshells). The RPA cross section is considerably higher than the RRPA ($4d + 5s + 5p$) cross section near threshold, presumably due to the different binding energies used in the two calculations. Indeed, for energies greater than 0.6 a.u. above threshold, where the use of different binding energies would not be as important as at threshold, the two calculations give virtually identical cross sections. It is interesting to note that the minimum in the cross section predicted by the RPA calculation is at the same energy (i.e., $\epsilon = 0.4$ a.u.) as predicted by both our length

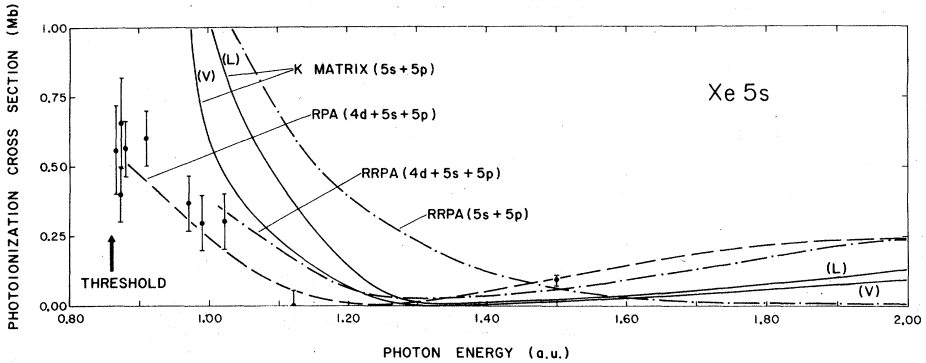


FIG. 3. Photoionization cross section for the 5s subshell of xenon plotted vs photon energy. Experimental data and theoretical results are indicated as in Fig. 2.

and velocity $K$-matrix calculations.

In Fig. 3 we have plotted the same theoretical calculations on a photon energy scale. Our results, as well as the RRPA results, are shifted with respect to the experimental data because of the differences between the corresponding theoretical binding energies and the experimental one (cf. Table II). The RPA results of Amusia and Cherepkov[18] are not shifted with respect to experiment because they have used the experimental binding energies in their calculation. It is difficult to decide whether it is better to present the theoretical results as in Fig. 2 or as in Fig. 3. On the one hand, when plotting the cross sections vs photoelectron energies in Fig. 2, the theoretical and experimental thresholds coincide. On the other hand, when plotting the cross sections vs photon energy as in Fig. 3, the theoretical and experimental cross sections refer to the same atomic transition energy. Clearly, however, all of the theoretical calculations describe the dynamics of the transition correctly; i.e., they all have a minimum in the cross section just above threshold. Figures 2 and 3 thus serve to illustrate the magnitude of relaxation effects resulting from the atomic transition, which to first approximation may be treated as a separate problem.

### B. Photoelectron angular distribution

Our length and velocity $K$-matrix ($5s+5p$) results for the photoelectron angular distribution asymmetry parameter are plotted in Fig. 4 as a function of photon energy. We find that $\beta$ obtains a minimum value of 1.8 at $\hbar\omega = 1.32$ a.u. in the velocity approximation and 1.91 at $\hbar\omega = 1.33$ a.u. in the length approximation. Not shown are $K$-matrix calculations we have performed in which correlations between the 5s and 5p subshells are ignored, that is, in which only final-state spin-orbit interactions are considered for the $5s \to \epsilon p$ transition. These latter calculations give results which are qualitatively similar to the Dirac-Fock results of Ong and Manson,[12,13] but which start at threshold with the value $\beta = 1.98$.

In comparison with the experimental measurements of Dehmer and Dill[1] and of White *et al.*,[45] our results for $\beta$ are too high. However, to achieve lower values of $\beta$ we would need larger values of the $^3P/^1P$ cross section ratio $r$ (cf. Table III), where $r$ is defined in terms of our calculated dipole amplitudes in Eq. (30). The difficulty in achieving higher values of the ratio $r$ is

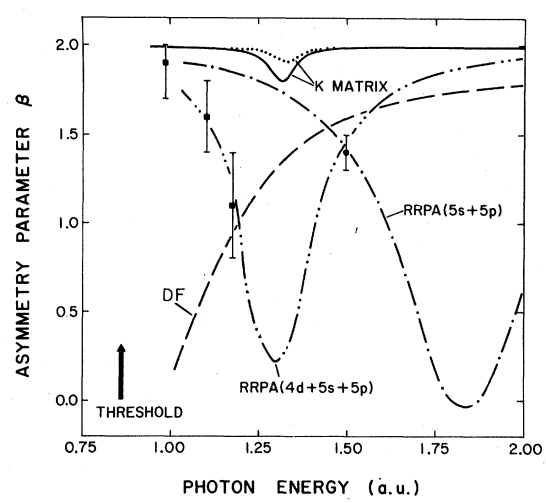


FIG. 4. Photoelectron angular distribution asymmetry parameter $\beta$. *K matrix*: present results including correlations between the 5s and 5p subshells in length (dotted line) and velocity (solid line) approximation. DF: Dirac-Fock independent-particle-model calculations of Ong and Manson (Refs. 12 and 13). RRPA: relativistic-random-phase-approximation calculations of Johnson and Cheng (Refs. 14 and 15) including correlations between the 5s and 5p subshells (dash-dot line) and between the 4d, 5s, and 5p subshells (dash-double dot line). *Solid circle*: Experimental results of White and Dill (Ref. 1). *Solid squares*: Experimental results of White *et al.* (Ref. 45). The arrow indicates the location of the experimental threshold energy.

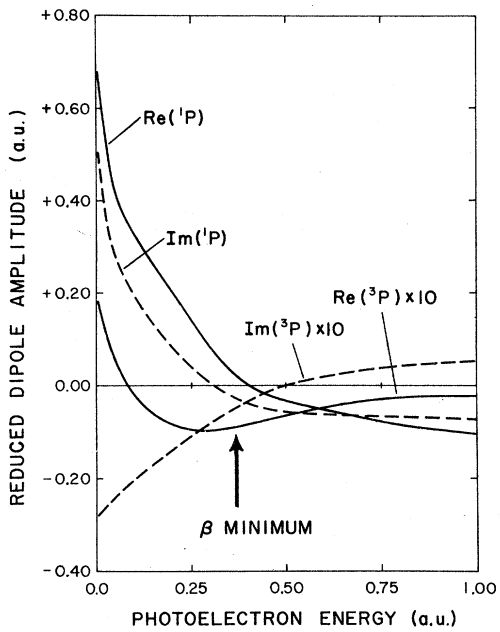


FIG. 5. Present $K$-matrix results for the real and imaginary parts of the reduced dipole amplitudes $D_E(^1P)$ and $D_E(^3P)$ in the velocity approximation. The arrow indicates the energy at which the corresponding asymmetry parameter $\beta$ has its minimum (i.e., $\epsilon = 0.37$ a.u.).

illustrated in Fig. 5, where we have plotted our results for the real and imaginary parts of the dipole amplitudes $D_E(^1P)$ and $D_E(^3P)$. We see that $|D_E(^1P)|^2$ never becomes zero (i.e., $r$ never becomes $\infty$) since the real and imaginary parts of $D_E(^1P)$ become zero at slightly different energies due to the details of the final-state correlations. Given, however, that our cross section results are in good agreement with experiment near the minimum in the cross section, we surmise that the reason our $\beta$-parameter results are not as low as experiment is that the magnitude of the forbidden-transition intensity $|D_E(^3P)|^2$ never becomes large enough near the minimum in $|D_E(^1P)|^2$.

The results of other relativistic theoretical calculations for $\beta$ are also shown in Fig. 4. The Dirac-Fock calculations of Ong and Manson[12,13] are independent-particle-model calculations which do not account for the correlations between the $5s$ and $5p$ subshells. Rather, they treat the following two transitions in $jj$ coupling,

$$\mathrm{Xe}\,5s^2 5p^6(^1S_0) + \hbar\omega \to \mathrm{Xe}^+\,5s_{1/2}5p^6\epsilon p_{1/2}(J=1) \to \mathrm{Xe}^+\,5s_{1/2}5p^6\epsilon p_{3/2}(J=1)\,, \qquad (40)$$

ignoring interchannel electrostatic correlations between the $\epsilon p_{1/2}$ and $\epsilon p_{3/2}$ final-state channels. If these latter interchannel correlations had been included, then their results would have been directly comparable to our results, not shown, in which we considered all final-state spin-orbit interactions between the following two transitions:

$$\mathrm{Xe}\,5s^2 5p^6 + \hbar\omega \to \mathrm{Xe}^+\,5s\,5p^6(^2S)\epsilon p(^1P_1) \to \mathrm{Xe}^+\,5s\,5p^6(^2S)\epsilon p(^3P_1)\,. \qquad (41)$$

As mentioned above, we found in these calculations that $\beta$ rises monotonically with energy from a threshold value of 1.98. This is in qualitative agreement with the Dirac-Fock results for $\beta$ of Ong and Manson,[12,13] which rise monotonically with energy from the much lower threshold value of 0.2. The Ong and Manson results are similar to the earlier Dirac-Slater results of Walker and Waber (not shown).[4]

The more detailed relativistic RPA calculations of Johnson and Cheng[14,15] are shown in two approximations in Fig. 4. These results for $\beta$ both agree with the experimental measurement of Dehmer and Dill,[1] but only those including correlations with the $4d$ subshell agree with the more recent measurements of White *et al.*[45] One sees that the minimum in $\beta$, which appears to be "below threshold" threshold in the DF calculations, is shifted to $\hbar\omega = 1.84$ a.u. (where $\beta = -0.04$) when correlations between the $5s$ and $5p$ subshells are taken into account and is shifted back to $\hbar\omega = 1.30$ a.u. (where $\beta = 0.21$) when correlations between the $5s$ and $4d$ subshells are also included. One might presume that the differences between our $K$-matrix ($5s+5p$) calculations and the RRPA ($5s+5p$) calculations of Johnson and Cheng[14,15] are mainly due to our neglect of the ground-state correlations that are treated in the random-phase approximation. However, unpublished calculations of Johnson and Cheng,[46] in which all final-state correlations between the $5s$ and $5p$ subshells were included but ground-state correlations were ignored, indicate that $\beta$ has a minimum value of $-0.17$ at $\hbar\omega = 1.65$ in the dipole velocity approximation and that $\beta$ has its minimum at a much higher energy in the dipole length approximation.

These detailed comparisons of our calculations with those of Ong and Manson[12,13] and with Johnson and Cheng[14,15,46] indicate that our use of nonrelativistic HF wave functions to describe the xenon core is probably responsible for the much shallower drop in $\beta$ that we obtain. All of these other calculations employed Dirac-Fock core orbitals. It should be stressed that the calculation of the forbidden $^3P$ transition amplitude is by its very nature difficult. Apparently, our calculations indicate that final-state spin-orbit interactions are not sufficient to obtain quantitatively good values for this amplitude. Our ne-

glect of ground-state correlations, of the influence of $5p \rightarrow \epsilon s$ transitions, and of correlations between the $4d$ and $5s$ subshells are not expected to change significantly the minimum values we obtain for $\beta$. They may, however, shift the location of the minimum in $\beta$. Nevertheless, the location of the minimum that we do obtain ($\hbar\omega = 1.32$ a.u.) is quite close to the result obtained in the best RRPA calculation ($\hbar\omega = 1.30$).

### C. Photoelectron spin polarization

Our $K$-matrix results for the photoelectron-spin-polarization parameters $\xi$, $\eta$, and $\zeta$, defined by Eqs. (36)–(38), are shown in Fig. 6. The predictions that these parameters give for the total photoelectron spin polarization $P$ [cf. Eq. (39)] produced by right circularly polarized light incident along the $Z$ axis is shown in Fig. 7. Given that our predictions for $|D_E(^3P)|$ are probably too small and that $\xi$, $\eta$, $\zeta$, and $P$ are all proportional to this forbidden amplitude, the large spin polarizations predicted in Fig. 7 are probably underestimated! However, we expect that our predictions are qualitatively accurate, especially since our predictions for the locations of the minima in the cross section and in the $\beta$ parameter are quite good. We note that Cherepkov[17] has predicted that $P$ achieves a maximum value of ≈100% by making *ad hoc* modifications of previous[18] nonrelativistic RPA results for the allowed dipole amplitude for the transition Xe $5s \rightarrow \epsilon p\,(^1P_1)$. Our predictions for $P$ agree qualitatively with those of Cherepkov.[17]

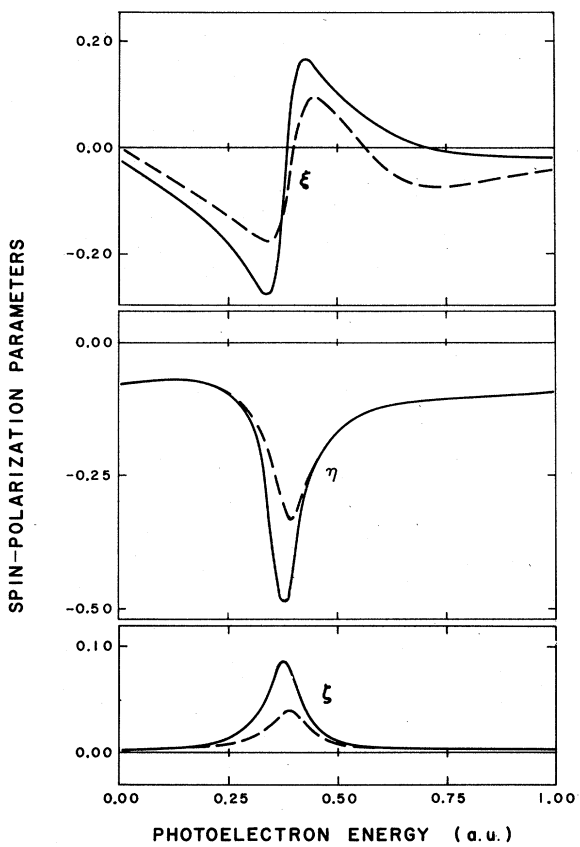


FIG. 6. Spin polarization parameters (dimensionless) $\xi$, $\eta$, and $\zeta$ for the Xe $5s \rightarrow \epsilon p$ transition as predicted by the present $K$ matrix ($5s + 5p$) calculation. Solid lines: velocity results. Dashed lines: length results.

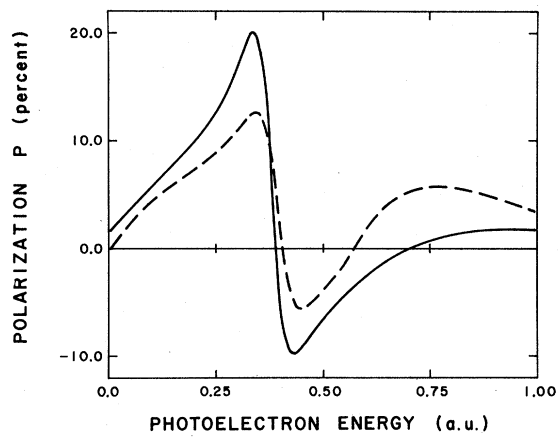


FIG. 7. Spin polarization $P$ along the $Z$ axis produced by right circularly polarized light incident along the $Z$ axis as predicted by the present $K$-matrix ($5s + 5p$) calculation. Solid line: velocity results. Dashed line: length results.

## VI. CONCLUSIONS

In our *ab initio* calculations we have examined the effects of final-state interchannel interaction and final-state spin-orbit interaction on experimentally measurable quantities associated with $5s$-subshell photoionization in xenon. The final-state spin-orbit interactions have been treated in the Breit-Pauli approximation as a perturbation on the nonrelativistic HF Hamiltonian. As expected, our predictions for the photoionization cross section are in good agreement with experiment near the minimum in the cross section. (Our neglect of correlations between the $5s$ and $4d$ subshells is the probable reason that our cross sections are too high just at threshold and too low at energies above the cross section minimum.) Our predictions for the asymmetry parameter $\beta$ and for the photoelectron spin polarization, however, appear to be only qualitatively correct due to the small values we obtain for the forbidden $^3P$ dipole transition amplitude. Since we have included all final-state relativistic interactions and since the electrostatic correlations are not necessary to obtain larger $^3P$ dipole amplitudes,

we conclude that our use of nonrelativistic core orbitals for the $Xe^+$ ion is the reason for the small forbidden-transition amplitudes that we obtain as compared to calculations employing Dirac-Fock wave functions. Despite our small values for the forbidden-transition amplitudes, our calculations predict quite large amounts of spin polarization near the 5*s*-subshell cross section minimum.

It is of interest to compare the present calculations with similar recent calculations[47] we have carried out for photoionization of the 6*s* electron in Cs:

$$\mathrm{Cs}\ 5p^6 6s\,(^2S_{1/2}) + \hbar\omega \rightarrow \mathrm{Cs}\ 5p^6(^1S_0)\epsilon p\,(^2P_{3/2,1/2})\,.$$

In Cs, final-state spin-orbit interactions cause the $J=\frac{3}{2}$ and $\frac{1}{2}$ final-state radial wave functions for the ejected electron to differ slightly. The result is that our calculations predict the angular distribution asymmetry parameter to drop from the value 2 to a minimum value of $-1$ and the spin polarization to approach 100% near the minimum in the 6*s*-subshell photoionization cross section. Since our calculations for these two atoms are very similar, especially in the treatment of final-state spin-orbit interactions, the difference in the results obtained (i.e., very dramatic relativistic effects in Cs as compared to rather subdued effects in Xe) may be traced to the different transitions studied. That is, in Cs the transition is an allowed one (i.e., $^2S \rightarrow {}^2P$) and the effect of spin-orbit interactions is to induce a "fine-structure" splitting between the $^2P_{3/2}$ and $^2P_{1/2}$ final states. In Xe, however, the final state has $J=1$ and the effect of spin-orbit interactions is to populate the *forbidden* transition $^3P_1$. Our calculations in this paper seem to indicate that forbidden transition amplitudes are much more difficult to calculate accurately than are the different fine-structure amplitudes for an allowed dipole transition.

Finally, we have pointed out the large discrepancies in the values of the subshell binding energies used in different theoretical approximations as well as their discrepancy with experimental values. These and other relaxation effects have concerned theoreticians for some time now.[19,20] Furthermore, it is of course possible, though laborious, to obtain theoretical predictions for binding energies that are in good agreement with experiment.[34] However, most theoretical calculations for transition amplitudes use simpler theoretical estimates for the associated binding energies, and experimentalists should be aware of the values used in trying to compare experimental measurements with theoretical predictions.

## ACKNOWLEDGMENTS

We are most grateful to Professor W. R. Johnson and Dr. K. T. Cheng for discussions concerning their work and for providing us with some of their results before publication. We also wish to thank Dr. R. A. Rosenberg, Dr. S. H. Southworth, and Professor D. A. Shirley for informing us of their recent experimental measurements of the Xe 5*s* $\beta$ parameter before publication. This research was supported in part by the U. S. Department of Energy under Contract No. EY-76-S-02-2892.A003. One of us (A.F.S.) wishes to acknowledge the support of the Alfred P. Sloan Foundation.

*Present address: Dept. of Physics, Univ. of Notre Dame, Notre Dame, Notre Dame, Ind. 46556.

[1]J. L. Dehmer and D. Dill, Phys. Rev. Lett. 37, 1049 (1976).
[2]C. N. Yang, Phys. Rev. 74, 764 (1948).
[3]This is not true for *s* subshells of open-shell atoms, however. See A. F. Starace, R. H. Rast, and S. T. Manson, Phys. Rev. Lett. 38, 1522 (1977).
[4]T. E. H. Walker and J. T. Waber, J. Phys. B 7, 674 (1974).
[5]H. A. Bethe and E. E. Salpeter, *Quantum Mechanics of One- and Two-Electron Atoms* (Springer-Verlag, Berlin, 1957), §§ 38–39.
[6]K.-N. Huang and A. F. Starace, Phys. Rev. A 18, 354 (1978).
[7]K.-N. Huang, Rev. Mod. Phys. 51, 215 (1979).
[8]U. Fano and J. W. Cooper, Rev. Mod. Phys. 40, 441 (1968). §6.
[9]A. F. Starace, "Theory of Atomic Photoionization," in *Handbuch der Physik*, edited by W. Mehlhorn (Springer-Verlag, Berlin, in press), Vol. 31.
[10]J. A. R. Samson and J. L. Gardner, Phys. Rev. Lett. 33, 671 (1974).
[11]K.-N. Huang and A. F. Starace, Bull. Am. Phys. Soc. 22, 1325 (1977).
[12]W. Ong and S. T. Manson, J. Phys. B 11, L65 (1978).
[13]W. Ong and S. T. Manson, Phys. Rev. A 19, 688 (1979).
[14]W. R. Johnson and K. T. Cheng, Phys. Rev. Lett. 40, 1167 (1978).
[15]W. R. Johnson and K. T. Cheng, Phys. Rev. A 20, 978 (1979).
[16]W. R. Johnson and C. D. Lin, Phys. Rev. A 20, 964 (1979).
[17]N. A. Cherepkov, Phys. Lett. A 66, 204 (1978).
[18]M. Ya Amusia and N. A. Cherepkov, Case Stud. At. Phys. 5, 47 (1975).

[19]G. Wendin, in *Photoionization and Other Probes of Many-Electron Interactions*, edited by F. J. Wuilleumier (Plenum, New York, 1976), pp. 61–82.
[20]M. Ya. Amusia, in *Atomic Physics 5*, edited by R. Marrus, M. Prior, and H. Shugart (Plenum, New York, 1977), pp. 537–565.
[21]C. Froese Fischer, Comput. Phys. Commun. 1, 151 (1969); 4, 107 (1972).
[22]G. N. Bates, Comput. Phys. Commun. 8, 220 (1974).
[23]K.-N. Huang, Phys. Lett. A 64, 39 (1977).
[24]H. P. Kelly, Phys. Rev. 136, B896 (1964); 144, 39 (1966).
[25]G. Breit, Phys. Rev. 34, 553 (1929).
[26]K.-N. Huang, Phys. Rev. A 18, 1119 (1978).
[27]Our single-electron radial continuum HF wave functions have the asymptotic form

$$\lim_{r\to\infty} R_{\epsilon l}(r) = (1/r)(2/\pi k)^{1/2} \times \sin[kr - \tfrac{1}{2}\pi l + k^{-1}\ln 2kr + \arg\Gamma(l+1-i/k) + \delta],$$

where

$$k = [2E(\text{a.u.})]^{1/2}$$

[28]G. Breit and H. A. Bethe, Phys. Rev. 93, 888 (1954).
[29]S. Altshuler, Nuovo Cimento 3, 246 (1956).
[30]A. F. Starace, Phys. Rev. A 2, 118 (1970).
[31]E. Clementi and C. Roetti, At. Data Nucl. Data Tables 14, 177 (1974).
[32]J. P. Desclaux, At. Data Nucl. Data Tables 12, 311 (1973).
[33](a) M. Aoyagi, M. H. Chen, B. Crasemann, K.-N. Huang, and H. Mark, Abstracts of the Fifth International Conference on Atomic Physics, Berkeley, California, 26–30 July 1976 (unpublished), pp. 300, 301. (b) K.-N. Huang, M. Aoyagi, M. H. Chen, B. Crasemann, and H. Mark, At. Nucl. Data Tables 18, 243 (1976).
[34]C. E. Moore, *Atomic Energy Levels* (U.S. GPO, Washington, D.C., 1958), Vol. III.
[35]The general angular-momentum-transfer analysis for photoionization of the 5*s* subshell of Xe is summarized in Ref. 1. In *LS* coupling one finds that angular-momentum transfers of zero correspond to $^1P$ transitions, while angular-momentum transfers of unity correspond to $^3P$ transitions.
[36]B. Brehm, Z. Phys. 242, 195 (1971).
[37]V. L. Jacobs, J. Phys. B 5, 2257 (1972).
[38]N. A. Cherepkov, Zh. Eksp. Teor. Fiz. 65, 933 (1973) [Sov. Phys. JETP 38, 463 (1974)]; J. Phys. B 11, L435 (1978); 12, 1279 (1979).
[39]C. M. Lee, Phys. Rev. A 10, 1598 (1974).
[40]K.-N. Huang, Phys. Rev. A (in press).
[41]Formulas (32)–(35) are equivalent to formulas (12), (13), (11), and (8), respectively, of Lee (Ref. 39) with the following change of notation: $\xi \to -\delta_k$, $\eta \to 2\xi_k$, and $\zeta \to \gamma_k$.
[42]D. J. Kennedy and S. T. Manson, Phys. Rev. A 5, 227 (1972).
[43]M. Ya. Amusia, V. K. Ivanov, N. A. Cherepkov, and L. V. Chernysheva, Phys. Lett. A 40, 361 (1972).
[44]T. Gustafsson, Chem. Phys. Lett. 51, 383 (1977).
[45]M. G. White, S. H. Southworth, P. Kobrin, E. D. Poliakoff, R. A. Rosenberg, and D. A. Shirley, Phys. Rev. Lett. 43, 1661 (1979).
[46]W. R. Johnson and K. T. Cheng (private communication).
[47]K.-N. Huang and A. F. Starace, Phys. Rev. A 19, 2335 (1979).